Electronic Supplementary Material (ESI) for Journal of Materials Chemistry A.

Supporting Information

Engineering Crystalline Structures of Two-Dimensional MoS_2 Sheets for High-Performance Organic Solar Cells

Xi Yang, Weifei Fu, Wenqing Liu, Jinghua Hong, Yu Cai, Chuanhong Jin, Mingsheng Xu*, Haibo Wang, Deren Yang and Hongzheng Chen*

Experimental Section

Chemically exfoliated MoS_2 nanosheets were synthesized through Li intercalation. 0.3 g pristine MoS_2 crystals (Sigma-Aldrich) were immersed in 3 mL of 1.6 M butyllithium solution in hexane for 2 days in glovebox. The $LixMoS_2$ was filtrated and washed with hexane to remove excess lithium and organic residues. Exfoliation was achieved immediately by ultrasonicating $LixMoS_2$ in water (10 mg/mL) for 2 h. Exfoliated MoS_2 solution was then dialyzed using MW 10,000 cut-off membranes for 5 days, followed by 4000 rpm centrifugation to remove any un-exfoliated aggregates. To prepare O-ce-MoS_2, the ce-MoS_2 ultrathin films were exposed to 3 min UV-ozone treatment.

Prior to device fabrication, the ITO substrates were cleaned by sonication using detergent, deionized water, acetone, and isopropanol sequentially for every 15 min followed by 15 min of ultraviolet ozone treatment. Then PEDOT:PSS (Baytron P AI4083) was spin-coated onto the cleaned ITO and annealed in air at 140 ^oC for 15 min. The ce-MoS_2 was spin-coated onto ITO for 3 times from a 2 mg/mL aqueous solution without further annealing. Then the substrates were transferred into a glovebox for spin coating of PTB7:PC_{71}BMactive layer with the thickness of about 90 nm.

Poly[(9,9-bis(3′-(N,N-dimethylamino)propyl)-2,7-fluorene)-alt-2,7-(9,9–dioctylfluorene)] (PFN) was deposited as electron transporting layer to extract electron to the cathode. Subsequently, samples were loaded into a vacuum deposition chamber (background pressure ≈ 5×10^{-4} Pa) to deposit 120 nm thick aluminum cathode with a shadow mask (device area of 4 mm^2). The J-V curves were measured with Keithley 236 measurement source units at room temperature in air. The photocurrent was measured under a calibrated solar simulator (Abet 300 W) at 100 mW cm^{-2}, and the light intensity was calibrated with a standard photovoltaic reference cell. External quantum efficiency (EQE) spectrum was measured with Stanford lock-in amplifier 8300 unit. Charge collection probability (P_C) was calculated by normalizing J_{ph} with $J_{ph,sat}$ ($J_{ph}/J_{ph,sat}$) from equations: $J_{ph,sat}$=qLG_{max}, J_{ph} =$qLG_{max}P_C$, where q is the elementary charge, L is the thickness of the active layer, and G_{max} is the maximum photoinduced carrier generation rate per unit volume. J_{ph} is calculated as J_{ph} = J_L-J_D, where J_L and J_D are the current density under illumination and in the dark, respectively. V_{int} is determined as V_{int} = V_{BI}-V_{app}, where V_{BI} is the built-in voltage, which refers to the voltage at which Jph is zero, and Vapp is the applied voltage.

TEM images were taken by a FEI TECNAI G2 F20-TWIN TEM and STEM images were taken by FEI Titan ChemiSTEM operated at 200 kV. The absorption spectra were recorded on a UV-Visible spectrophotometer (UV-2450, Shimadzu Corporation, Japan). The AFM images were taken by a Veeco Multimode atomic force microscopy in the tapping mode. The steady-state photoluminescence PL spectra were taken on a HORIBA Jobin Yvon FluoroMax-4 spectrofluorometer. Raman spectra were recorded on inVia Raman microscope. XPS and UPS measurements were conducted using an ESCALAB 250Xi (Thermo) system.

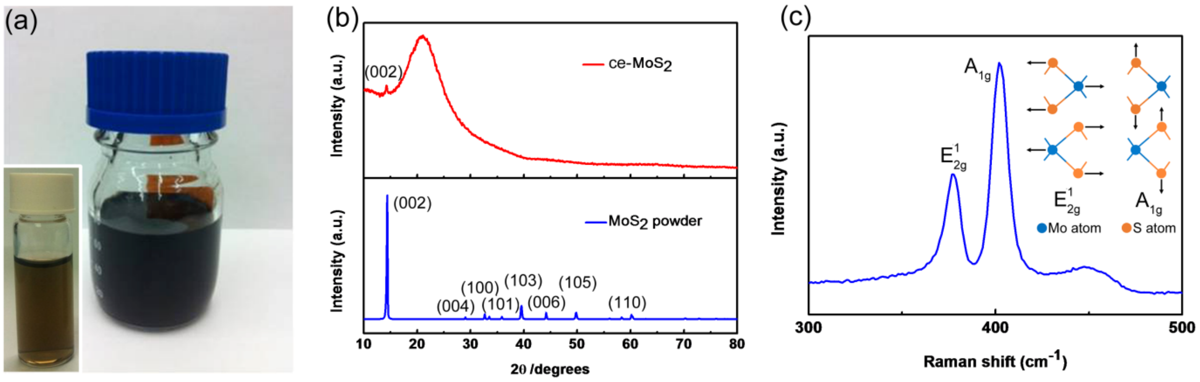

Figure S1. (a) Photograph of the as-prepared ce-MoS_2 colloidal suspension in water. Inset shows the diluted ce-MoS_2 sheet suspension with a dark yellow color. (b) Powder X-ray diffraction (XRD) patterns of bulk MoS_2 powder and ce-MoS_2 nanosheets. The samples were deposited on quartz substrates for testing. (c) Raman spectrum of ce-MoS_2 thin films deposited on SiO_2/Si substrate. The inset in (c) shows the atomic displacements for the in-plane phonon mode E^1_{2g} and the out-of-plane phonon mode A_{1g} for two adjacent layers.

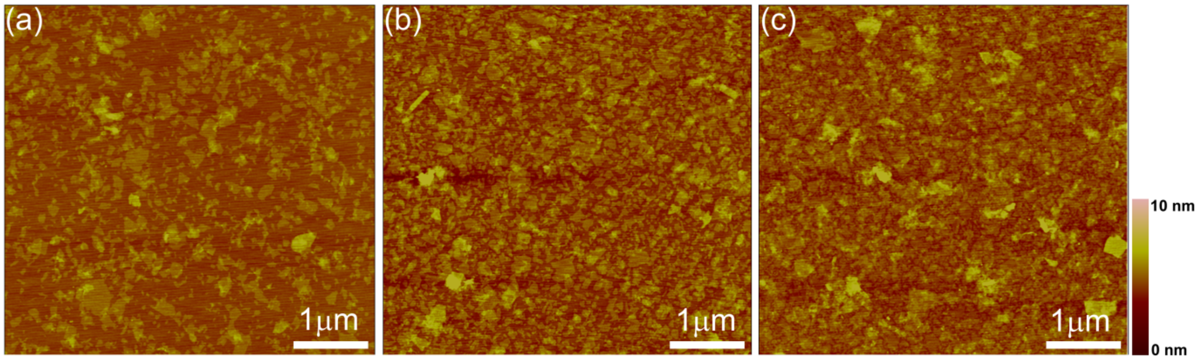

Figure S2. AFM images of ce-MoS_2 thin film deposited on SiO_2/Si substrate. The ultrathin film of ce-MoS_2 sheets was deposited by multiple-step spin-coating from 2mg/ml ce-MoS_2 aqueous colloidal suspension: (a) 1-time spin-coating; (b) 2-time spin-coating; (c) 3-time spin-coating. We found that by spin-coating 3 times on SiO_2/Si, ce-MoS_2 sheets can fully cover the whole substrate as shown in this image. The thickness of monolayer MoS_2 sheet is about 1 nm, and most area of the film is composed of 2 or 3 layers of MoS_2. Thus, our ce-MoS_2 used in OSCs was estimated to be 2-3 nm after spin-coating of 3 times. For the device fabrication in this work, ce-MoS_2 was deposited on ITO under the same spin-coating conditions.

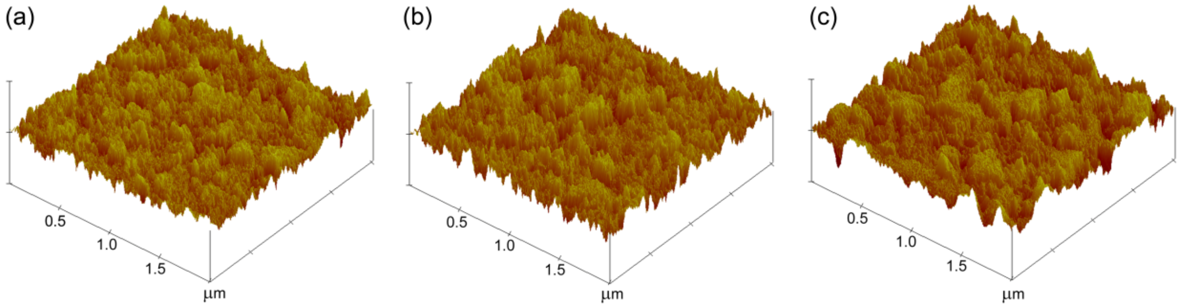

Figure S3. Three-dimensional topography images of (a) bare ITO, (b) ce-MoS_2 ultrathin film on ITO, and (c) O-ce-MoS_2 ultrathin film on ITO. The 2 nm MoS_2 thin film is difficult to be seen on ITO through AFM because of the very rough ITO surface. The AFM images of MoS_2 thin film on ITO show no difference to the bare ITO surface, indicating the successful controlling the MoS_2 film on ITO to be an ultrathin layer. No difference was observed before and after O incorporation. It means the UV-ozone treatment would not change the morphology of ce-MoS_2 thin film.

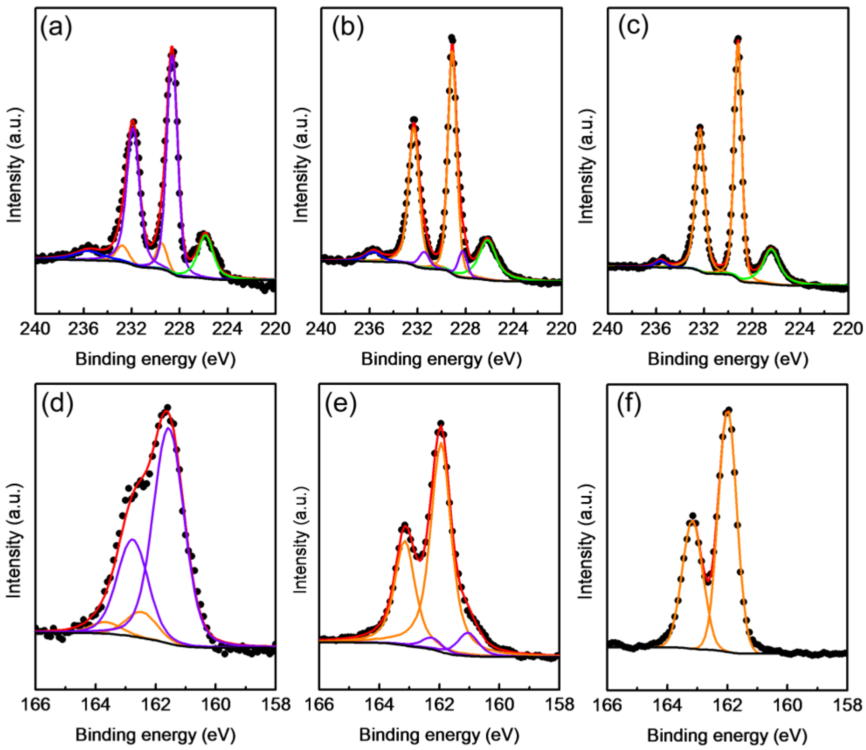

Figure S4. XPS spectra showing Mo3d, S2s, and S2p core level peak regions for ce-MoS_2 thin films annealed at 0 °C (a,d) 150°C (b,e) and 300°C (c,f). After Shirley background subtraction, the Mo3d and S2p peaks were deconvoluted to show the 2H and 1T contributions, represented by orange and violet plots, respectively. Annealing was conducted in a golvebox to prevent oxidation.

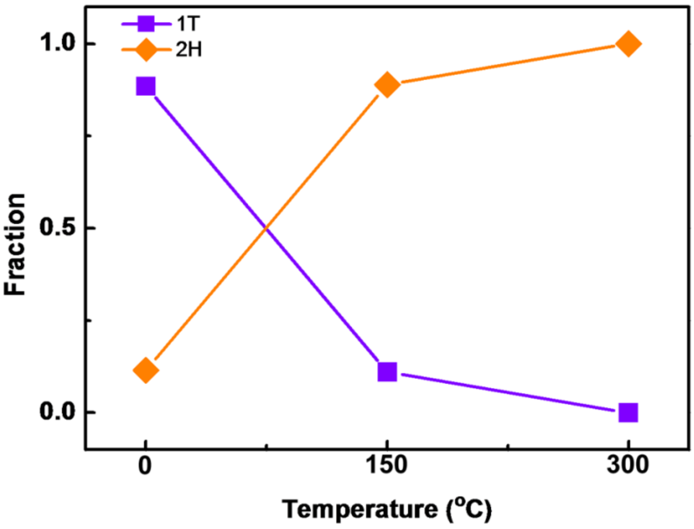

Figure S5. Extracted relative fraction of 2H and 1T components as a function of annealing temperature.

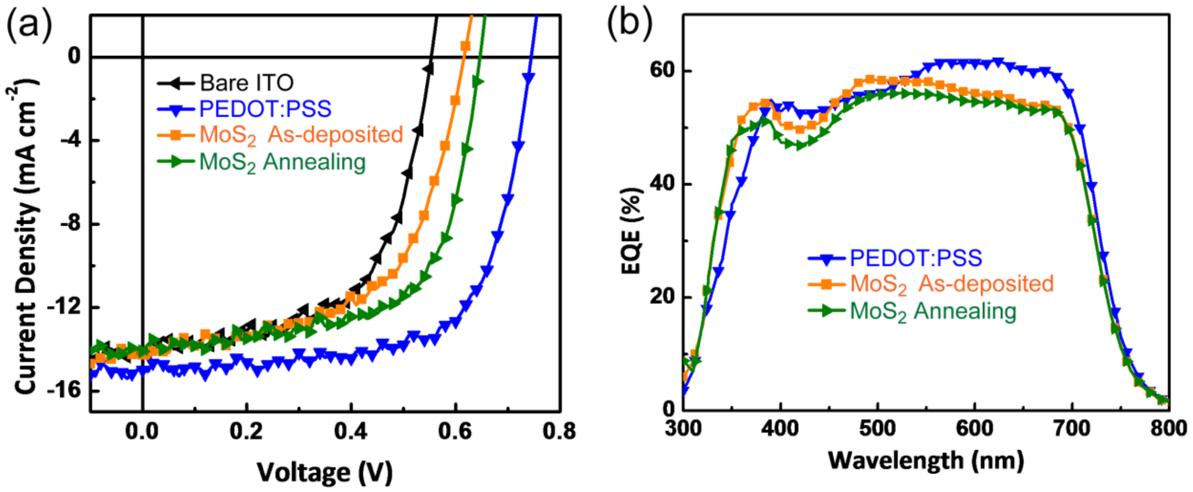

Figure S6. (a) *J-V* characteristics and (b) external quantum efficiency (EQE) spectra of the OSC devices with bare ITO, PEDOT:PSS, ce-MoS$_2$ and 150 °C annealed ce-MoS$_2$ as hole extraction layers, respectively, under AM 1.5G illumination (100 mW cm^{-2}). The annealing time is 15 min (in the glovebox to avoid oxidization). Compared to as-deposited ce-MoS$_2$, annealing can slightly improve the device performance to 5.77% PCE with a V$_{OC}$, J$_{SC}$, and FF of 0.65 V, 14.10 mA cm^{-2}, and 0.63, respectively.

Table S1. Performance of the OSC devices with bare ITO, PEDOT:PSS and ce-MoS$_2$ as hole extraction layers, respectively, under AM 1.5G illumination (100 mW cm^{-2}). The ce-MoS$_2$ thin films with different treatments (as-deposited, annealing at 150 °C, and 300 °C in the glovebox) were investigated.

Anode buffer layer	Treatment	Voc [V]	Jsc [mA cm^{-2}]	FF	PCE [%]
Bare ITO	-	0.55	14.14	0.591	4.60
PEDOT:PSS	Annealing	0.74	15.00	0.685	7.60
ce-MoS$_2$	As-deposited	0.62	14.29	0.563	4.99
	150 °C Annealing	0.65	14.10	0.630	5.77
	300 °C Annealing	0.56	13.83	0.616	4.77

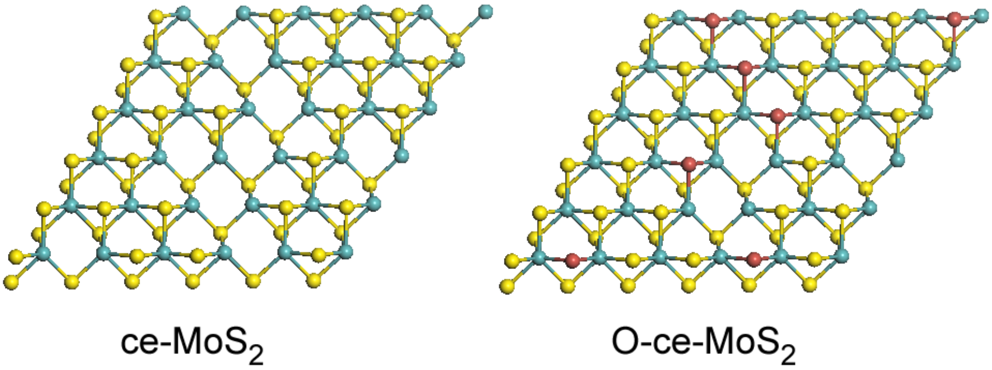

Figure S7. Schematic drawings of the single layer ce-MoS_2 and O-ce-MoS_2.

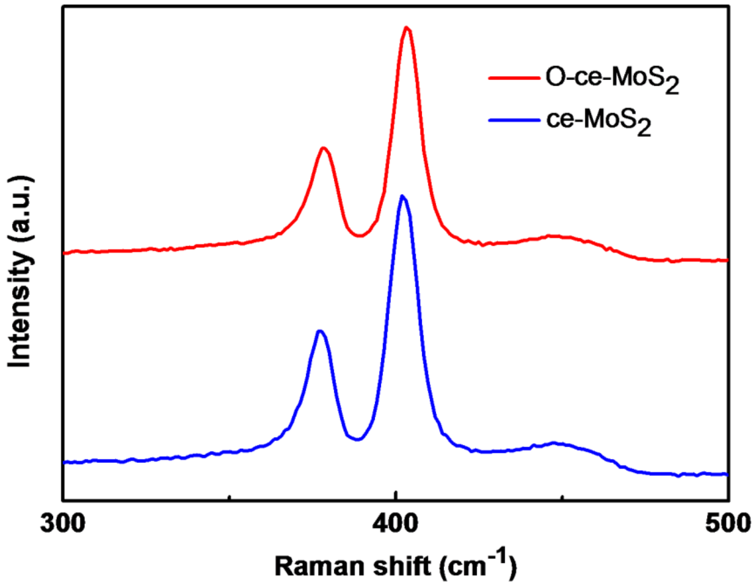

Figure S8. Raman spectra of ce-MoS_2 and O-ce-MoS_2 thin films deposited on SiO_2/Si substrates.

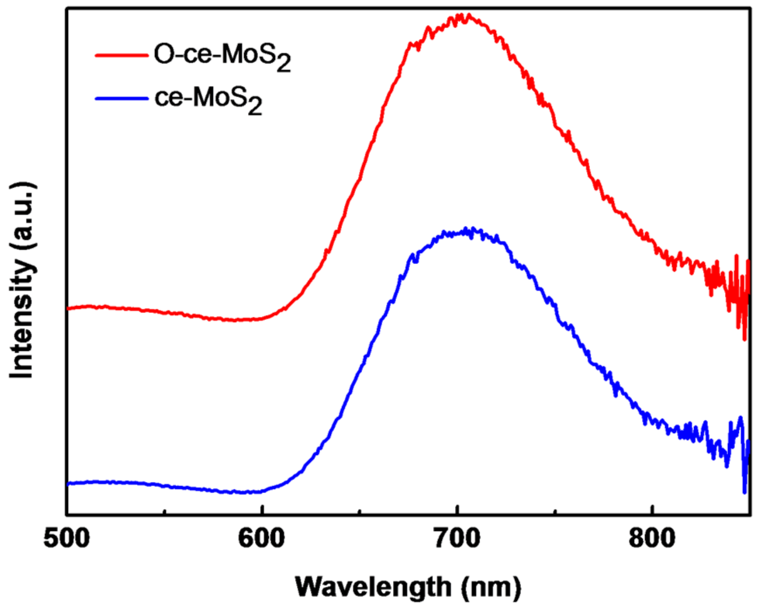

Figure S9. Photoluminescence spectra of ce-MoS_2 and O-ce-MoS_2 thin films.

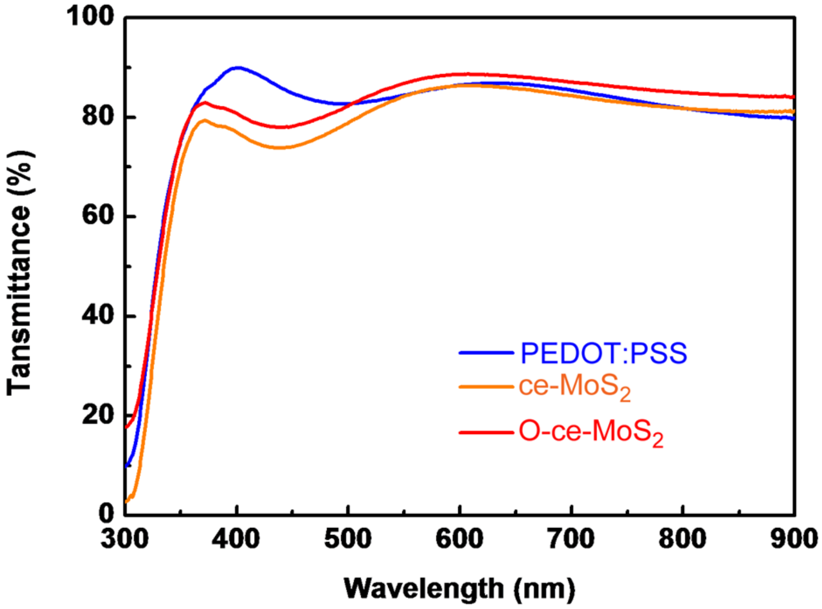

Figure S10. Transmission spectra of PEDOT:PSS, ce-MoS_2 ultrathin film, and O-ce-MoS_2 ultrathin film. All the samples were deposited on cleaned ITO substrates. High transparency are achieved across a wide range of the visual spectrum for both ce-MoS_2 and O-ce-MoS_2, which are comparable to that of PEDOT:PSS.